

Efficient removal of amoxicillin antibiotics onto magnetic graphene oxide: adsorption performance, mechanism, and regeneration exploration

Sulieman Ibraheem Shelash Al-Ha-Wary, Reena Gupta, I. B. Sapaev, Khulood H. Oudaha, Mays Jassim Abdalkareem, Ali Alsalamy, Ahmed Hussien Radie Alawadi, Fatemeh Zisti, Hossein Moein & Davoud Balarak

To cite this article: Sulieman Ibraheem Shelash Al-Ha-Wary, Reena Gupta, I. B. Sapaev, Khulood H. Oudaha, Mays Jassim Abdalkareem, Ali Alsalamy, Ahmed Hussien Radie Alawadi, Fatemeh Zisti, Hossein Moein & Davoud Balarak (17 Oct 2023): Efficient removal of amoxicillin antibiotics onto magnetic graphene oxide: adsorption performance, mechanism, and regeneration exploration, International Journal of Environmental Analytical Chemistry, DOI: [10.1080/03067319.2023.2266698](https://doi.org/10.1080/03067319.2023.2266698)

To link to this article: <https://doi.org/10.1080/03067319.2023.2266698>



Published online: 17 Oct 2023.



Submit your article to this journal [↗](#)



View related articles [↗](#)



View Crossmark data [↗](#)



Efficient removal of amoxicillin antibiotics onto magnetic graphene oxide: adsorption performance, mechanism, and regeneration exploration

Sulieman Ibraheem Shelash Al-Ha-Wary^a, Reena Gupta^b, I. B. Sapaev^c,
Khulood H. Oudaha^d, Mays Jassim Abdalkareem^e, Ali Alsalamy^f,
Ahmed Hussien Radie Alawadi^g, Fatemeh Zisti^h, Hossein Moeiniⁱ and Davoud Balarakⁱ

^aBusiness Management, Department of Business Administration, Business School, Al al-Bayt University, Mafraq, Jordan; ^bInstitute of Pharmaceutical Research, GLA University Mathura, Mathura, UP, India; ^cTashkent Institute of Irrigation and Agricultural Mechanization Engineers, National Research University, Tashkent, Uzbekistan; ^dPharmaceutical Chemistry Department, College of Pharmacy, Al-Ayen University, Thi-Qar, Iraq; ^eDepartment of Medical Laboratory Technologies, Al Rafidain University College, Bagdad, Iraq; ^fCollege of Technical Engineering, Imam Ja'afar Al-Sadiq University, Al-Muthanna, Iraq; ^gMedical Laboratory Technology Department, College of Medical Technology, Islamic University, Najaf, Iraq; ^hDepartment of Chemistry, University of Brock, St. Chatarines, Ontario, Canada; ⁱDepartment of Environmental Health, Health Promotion Research Center, Zahedan University of Medical Sciences, Zahedan, Iran

ABSTRACT

The present study was done to synthesise an adsorbent, i.e. magnetic graphene oxide (MGO) nanocomposite, which was performed based on a facile precipitation method and was utilised in experiments for removing amoxicillin (AMX). The characteristics of the prepared adsorbent were defined based on commonly utilised analyses (SEM, XRD, BET, TEM, FTIR, VSM, and pH_{pzc}). According to kinetic studies, the PSO model was found as an applicable model for describing data. Moreover, the two-step diffusion process, i.e. diffusion in the boundary layer and the porous structures, was perceived for the evaluated process based on the IPD model. The isotherm models, including Langmuir, Freundlich, Temkin, and D–R, were employed for fitting data and calculating AMX adsorption capacity, among which Langmuir was the best one; using this model, the maximum adsorption capacities for MGO were 91.4, 103.9, 112.3, and 122.5 mg/g, which were achieved at 20, 30, 40, and 50°C. In addition, a feasible, spontaneous, and endothermic process was found for the adsorption of AMX ions, according to thermodynamic studies. The highest percentage of removal (100%) was obtained for the initial concentration of 25 mg/L at 50°C using the adsorbent dose of 1.5 g/L at a pH of 5 and a contact time of 90 min. The values of 74.4 m^2/g and 27.74 emu/g were detected for the specific surface area and saturation magnetisation values of the MGO, respectively. The overall results were representative of the suitability of the MGO as an adsorbent for removing AMX from aqueous media.

ARTICLE HISTORY

Received 31 July 2023
Accepted 24 September 2023

KEYWORDS

Amoxicillin; magnetic graphene oxide; adsorption isotherm; adsorption kinetics; thermodynamic

1. Introduction

This century has been associated with environmental pollution as a crucial problem that has been aroused from technological progress [1,2]. At the beginning of the twentieth century, antibiotics for curing the disease were replaced with the traditional way for this purpose; plants and moulds with antibiotic-like properties have been common substances used by different cultures of the ancient era for treating the disease [3,4]. As an extensively used drug in treating humans and animals, antibiotics have recently become a serious concern due to their pollution potential, which is aroused from excreting a large fraction of the un-metabolised form of these substances [5,6].

The entrance of the mentioned compounds through wastewater of pharmaceutical companies and hospitals into surface or underground water has been found to be associated with severe hazards. In addition to the fact that they are a threat to the environment, the risk of microorganism resistance after their release into the environment is considered another important risk; this leads to the loss of their curing properties and the incidence of another problem due to microorganism resistance [7,8].

An extensively used compound of this group is AMX (a broad-spectrum beta-lactam antibiotic belonging to the penicillin class). It is utilised for treating gastrointestinal and systemic infections caused by bacteria [9]. Human prescription of this antibiotic is also done against bacterial infections. Considering the recent reports on domestic wastewater and industrial wastewater, concentrations in the range of ng/L to mg/L have been detected [10]. Toxic effects might be induced by this antibiotic since it has a resistance and bioaccumulation nature in the environment, which can lead to changes in the natural balance of ecosystems [11]. Based on the given information, treating the effluents containing AMX should be considered as an important subject before its discharge into the environment [12]. Removing AMX from wastewater has been evaluated using ion exchange, biological degradation, and adsorption using various kinds of adsorbents, etc., among which the adsorption process has found an extensive application for removing the pollutants [13]. In the application of the adsorption process, choosing an adsorbent with high efficiency and quick and easy separation after installation are two major challenges [14]. Active granulated carbons have been found as highly used adsorbing materials; however, there are problems in their application in terms of cost and regeneration [15]. Among the types of adsorbents, graphene oxide has a single-layer structure of carbon with a significant active surface, which is found densely and in the form of a crystalline honeycomb network [16].

Graphene is a unique form of carbon made up of a single layer of carbon atoms arranged in a hexagonal pattern [17]. It has a small overlap between the valence and conduction bands and is known as a semi-metal. In other allotropes of carbon (e.g. graphite, diamond, charcoal, carbon nanotubes, and fullerenes), this semi-metal exhibits a role as the basic structural element [18]. Graphite, when oxidised, can generate graphene oxide (GO), which boasts a single-atomic-layered structure. GO readily disperses and dissolves in numerous solutions, including water [19]. On the GO surface, epoxide, carboxyl, and hydroxyl groups are present [20]. In addition, this substance has a superior specific surface area, which has attracted remarkable attention for its application as an adsorbent for eliminating different pollutants in water and wastewater sources [21,22]. However, suffering from a

drawback, i.e. the separation after utilising in the adsorption process, has been reported based on conducted studies [23]. There are methods for its separation from a solution such as filtration and centrifugation, but these methods have been found to be associated with issues in terms of cost, energy, and manpower losses [24]. Thus, we magnetised the GO in the present study to facilitate its separation.

Since MGO has a magnetic feature, there is a significant simplicity in its separation after adsorption [25]. Nonetheless, its adsorption sites have been occupied by pollutants, which restricts its direct reuse after separation and implies the need for a well-organised method for its regeneration [26]. In this case, a possible choice is thermal regeneration, which is restricted by high energy costs due to the need for high temperatures. Another environmentally friendly option known for this purpose is the biological regeneration method; however, the use of this method is generally limited due to the long operation time caused by its low rate [27,28]. In addition, the utilisation of inorganic (acid, alkali, etc.) or organic solvents (ethanol, acetone, etc.) for washing has been found as another method for the regeneration of MGO; this method has also been found to be associated with drawbacks so that additional organic pollution is produced during the use of organic solvents, and large amounts of spent washing water are generated when washing process is done by inorganic solvents [29,30].

One of the recently utilised methods for the regeneration of adsorbent is the advanced oxidation process (AOP) based on persulphate (oxidation agents, e.g. peroxymonosulfate (PMS) and peroxydisulfate (PDS)) [31]. PMS has been found to be more effective than PDS in the mineralisation of pollutants due to having more activity raised by its asymmetric structure [32]. Utilising magnetic graphene-based materials in AOP has been associated with acceptable results in degrading pollutants. However, the water matrix features (e.g. inorganic ions and natural organic matter) have been found to be effective on persulphate-based AOP [33]. Furthermore, there was evidence of adverse effects associated with the direct use of persulphate-based AOP on the water quality, which is raised by the discharge of sulphate anions [34]. According to available documents, the use of the mentioned system, i.e. persulphate-based AOP has been capable of providing suitable results for the regeneration of activated carbons so that it has become an eye-catching approach in this case [35]. Since the MGO has the catalytic ability, PMS activation in the presence of spent MGO can lead to the remarkable success of the regeneration process. Hence, a decrease in energy inputs is expected, which leads to the cost-effectiveness of the persulphate-based regeneration method [36].

Hence, MGO, as our desired adsorbent for removing AMX from the aqueous solution, was synthesised using the facile co-precipitation method. To provide detailed information on our conducted study, examining the isotherms, kinetics, and thermodynamics of adsorption and evaluating the effects of reaction temperature, contact time, pH, adsorbent, and AMX mass were also considered as sub-objective of the present study. The properties of the adsorbent were fully investigated. The effects of anions and cations were also done in this study. In addition to the regression coefficient, four error models were used to determine the isotherm and kinetics. Furthermore, the MGO was undergoing PMS oxidation at ambient temperature for evaluation of its regenerability.

2. Materials and methods

2.1. Reagents

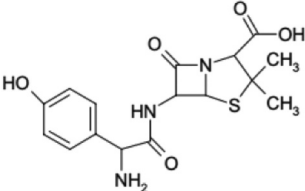
Analytical purity of Amoxicillin (AMX) was provided by Sigma-Aldrich (St Louis, MO, 82 USA). After preparing the AMX stock solution, the desired concentrations were diluted using distilled water. The list of all the materials and devices, which were employed in this study is seen in Table 1.

2.2. Preparation of graphene oxide

The Staudenmaier method was used for the synthesis of graphene oxide in this study [21]. In addition, its schematic is shown in Figure 1. The working method is as follows: 1 g of graphite powder was added to a 50 ml Erlenmeyer flask containing 18 ml of sulphuric acid and 9 ml of nitric acid in an ice bath at 0°C and mixed completely. 10 g of potassium chlorate powder was added to the resulting sample and placed in a shaker at 0°C for 1 h. Then, the sample was placed on a shaker for an hour at room temperature and mixed completely. The obtained mixture was washed with double distilled water to neutralise the pH of the sample. The resulting material was dried in an oven at a temperature of 60°C, and at the end, the sample was ultrasonicated in a solution of water and ethanol with a volume ratio of 50% for two hours. In order to separate graphene oxide, a centrifuge with a speed of 3000 rpm was used for 15 min.

In order to produce iron oxide, 1.25 g of FeCl₂ and 2.5 g of FeCl₃ in a volumetric flask were brought to a volume of 150 ml with double distilled water and thoroughly stirred by a shaker at a temperature of 50°C. 12.5 ml of ammonia was slowly added to the sample. Then, the resulting sample was collected, washed with double distilled water and ethanol, and dried in an oven at 60°C for one hour. Then, 2 mg of Fe₃O₄ and 2 mg of graphene oxide were mixed in 20 ml of double distilled water and stirred in a shaker for 4 h. Magnetic graphene oxide was collected using a magnet, and finally, the sample was dried in an oven at 60°C. For the PMS oxidation method, the magnetically separated spent

Table 1. List of instruments and materials.

Parameter	Character/Value
Molecular structure	
CAS number: 26787-78-0	
Molecular formula: C ₁₆ H ₁₉ N ₃ O ₅ S	
Molecular weight: 365.4 g/mol	
Solubility in water: 3430 mg/L at 20°C	
Acid dissociation constant (pKa): 2.4 (carboxyl), 7.4 (amine) and 9.6 (phenol)	Merck Group, Germany
Sodium hydroxide (NaOH, ≥98%), hydrochloric acid (HCl, 37%) and ammonium chloride (NH ₄ Cl, 30%). Sulfuric acid (H ₂ SO ₄ , ≥98%), Nitric acid (HNO ₃ , ≥65%), Potassium chlorate (KClO ₃ , ≥70%), Iron(II) chloride (FeCl ₂ ·4 H ₂ O), Iron (III) chloride (FeCl ₃ ·6H ₂ O), CaCl ₂ ·6H ₂ O, M ₃ SO ₄ ·7H ₂ O, NaNO ₃	
TEM	ZEISS LEO 912 AB
XRD	A PHILIPS, PW1800 (Netherland)
VSM	MDKFD instrument (Iran)
Scanning electron microscope (SEM)	TESCAN MIRA3, Czech Republic
pH meter	HANNA (model 211)
Fourier-transform infrared spectroscopy	Nicolet 6700 FT-IR

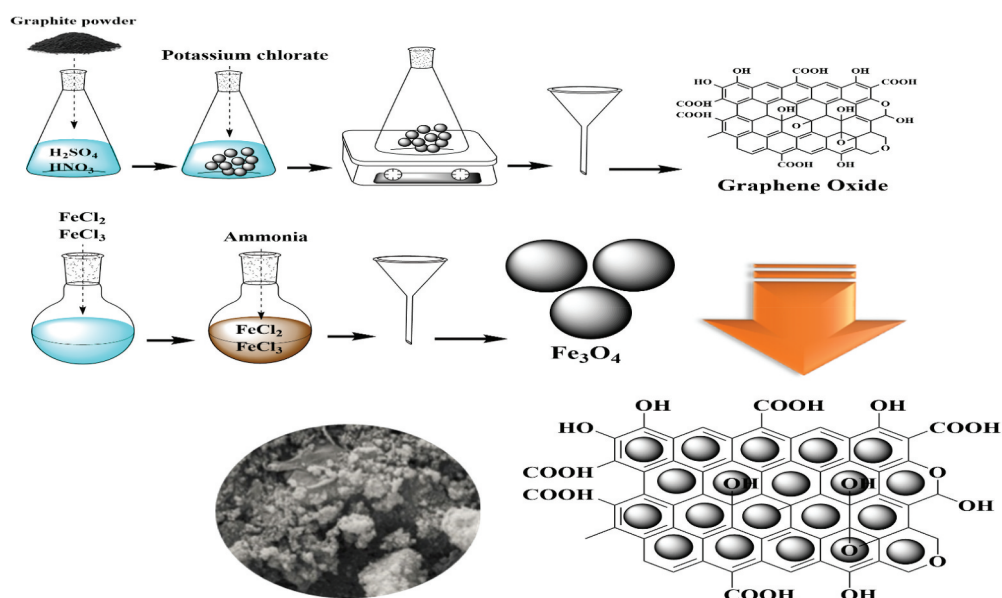


Figure 1. Schematic of synthesis of MGO by co-precipitation method.

adsorbent was treated with 25 mL of 2-mM PMS for 2 h, washed with 25 mL of water to remove residual PMS, and then used for the next run.

2.3. Batch adsorption

200 mL glass flasks were employed for adsorption batch tests ($30 \pm 2^\circ\text{C}$); in these flasks, there was 100 mL of AMX solution with different concentrations prepared in distilled water. After adding MGO adsorbent (1.5 g) to the flask, a 150 minute-stirring process using an orbital shaker was considered at 120 rpm. The $\text{pH} = 5$ was considered as the pH of the solution under study. The pH of the samples was adjusted using HCl and NaOH (0.1 N). When the adsorption process finished, several samples were withdrawn and analysed in terms of AMX concentration. The studies were conducted in a known time range (0–150 min). Separation of MGO from solutions was first done using a magnet. After that, to ensure the complete MGO separation and avoid the interference of its fines in the analysis, a $0.45 \mu\text{-cellulose}$ filter was used.

The pH at the point of zero charge (pH_{pzc}) is an important parameter to get a better understanding of the surface adsorption mechanism. The pH_{zpc} of the adsorbent was carried out using the simple solid addition method [25]. In brief, a solution of 0.2 mol/L NaCl was prepared and boiled to remove dissolved CO_2 and then cooled to room temperature. The initial pH (pH_i) of this solution was adjusted from $\text{pH} 2$ to 12 by adding either 0.1 mol/L HCl or 0.1 mol/L NaOH. MGO (0.2 g) was added to 100 mL of 0.1 mol/L NaCl solution in 100 mL conical flasks and stirred in a shaker at 180 rpm. Then, the final pH (pH_f) of the solution was measured. The graph was plotted between the difference between the final and initial pH ($\text{pH}_f - \text{pH}_i$) against the initial pH (pH_i), and the point of intersection of the two graphs was taken as the pH_{zpc} of the MGO.

In this study, kinetic (PFO, PSO, and IPD) and isotherm models (Langmuir, Freundlich, Temkin, and D-R) were utilised for describing data. Moreover, thermodynamic studies were done based on calculating the ΔG° , ΔH° , and ΔS° .

In the case of all samples, determining their AMX concentration was carried out using HPLC (C₁₈ ODS column) with a UV detector 2006 at 190 nm. A mixture of buffer phosphate (pH = 4.8) and acetonitrile (a volumetric ratio of 60/40) was the mobile phase. The injection flow rate was considered as 1 mL/min.

The following equations were the basis of determining the adsorption capacity (q_e) and removal efficiency (R) of AMX (Equations (1) and (2)) [37]:

$$Q_e = \frac{(C_0 - C_e)V}{M} \quad (1)$$

$$\%R = \frac{(C_0 - C_e)}{C_0} \times 100 \quad (2)$$

2.4. Validity of adsorption isotherm and kinetic model

To confirm the fit model for the adsorption system, in addition to the regression coefficient, it is necessary to use error analysis for more emphasis. The calculated expressions of some error functions were determined using Equations (3)–(6) [38]:

$$SSE = \sum (q_c - q_e)^2 \quad (3)$$

$$SAE = \sum |(q_c - q_e)^2| \quad (4)$$

$$ARE = \frac{(\sum |(q_c - q_e)/q_e|)}{n} \quad (5)$$

$$ARS = \sqrt{\frac{\sum [(q_c - q_e)/q_e]^2}{n - 1}} \quad (6)$$

Where n is the number of experimental data points, q_c is the predicted (calculated) quantity of AMX adsorbed onto MGO according to the isotherm equations, and q_e is the experimental data.

3. Results and discussion

3.1. Adsorbent specifications

As depicted by FTIR spectra in Figure 2(a), at approximately 3572 and 1590 cm^{-1} , there are broad bands in all the samples, which are ascribed to the stretching and bending vibrations of -OH groups [22]. Moreover, in the GO patterns, a peak at 1692 cm^{-1} ascribed to the stretching vibration of C=O groups was detected, and in the pattern of Fe₃O₄, there were two peaks at 677 and 580 cm^{-1} attributed to Fe–O bonds. In addition, the presence of those peaks for GO and Fe₃O₄ in the pattern of MGO with reduced intensities was

confirmed by FTIR results; based on this, we can express that composite material has been prepared fruitfully. Additional bands, which have been appeared after the AMX adsorption, were recognised at 1608, 1325, 1229, and 1135 cm^{-1} [24]. These bands were identified as the C–N stretching vibration of the heterocycle, the C–N stretching vibration of the terminal dimethylamino group, and the C–C stretching and bending vibrations of the heterocycle [21]. Based on this, it can be confirmed that AMX was indeed adsorbed on the adsorbent.

Using VSM at room temperature, Fe_3O_4 nanoparticles and MGO were evaluated in terms of magnetic properties. As seen in Figure 2(b), a superparamagnetic characteristic is detectable for MGO based on near-zero remanence and coercivity at room temperature. The values of 72.95 emu/g and 27.74 emu/g were obtained as saturation magnetisation values for Fe_3O_4 nanoparticles and MGO, respectively. As perceived, the saturation magnetisation value for MGO was decreased, which indicates that the magnetic property of Fe_3O_4 was decreased due to the existence of loaded GO. However, excellent magnetic sensitivity was still detectable for MGO (Figure 2(b)), so that separating AMX-loaded adsorbent from the solution is easily possible using a magnet within 15 s. Our observation confirms the facile separability of MGO, which enhances its applicability.

SEM technique (Figure 2(c,d)) used for determining the size and shape of the synthesised GO and MGO nanoparticles was representative of the flaky texture of natural GO; this is related to the layered nanostructure of GO. In addition, the successful synthesis of MGO is confirmed based on Figure 2(d), which represents the coating of the outside surface of GO layers with spherical Fe_3O_4 .

For defining the morphology of GO, we used the TEM measurements; based on this (Figure 2(e)), a typical sheet-like morphology with wrinkles was detected for GO, and the sheets have a transparent nature, which is indicative of the exfoliation of GO to monolayer or few-layer structures. Moreover, considering Figure 2(f), which represents the MGO image, there are aggregates of spherical particles; these aggregates appeared after applying the coprecipitation process for synthesising MGO.

In the nitrogen adsorption – desorption isotherm, we can detect the unique hysteresis loops (Figure 2(g)); according to IUPAC classification, these are of type IV. BET examination was indicative of the specific surface area of $74.4\text{ m}^2/\text{g}$ for the MGO. In addition, determining pore size was done based on The Barrett – Joyner–Halenda (BJH) technique. The dominance of mesoporous in MGO was confirmed based on the sharp peak at 31 nm in the curve obtained by drawing the pore volume versus pore diameter.

The XRD patterns of GO, Fe_3O_4 NPs, and MGO samples before and after recycling are shown in Figure 3. It is evident that all samples (Except for GO) have the typical XRD pattern of magnetite (JCPDS No. 19–0629), indicating that the Fe_3O_4 NPs retain their original crystalline structure. XRD pattern of GO has a strong diffraction peak at $2\theta = 11.6^\circ$, which originated from the diffraction on its (001) layer planes. For Fe_3O_4 nanoparticles, all diffraction peaks in the XRD pattern at $2\theta = 30.29^\circ, 35.81^\circ, 43.31^\circ, 53.85^\circ, 56.79^\circ, 63.1^\circ,$ and 75.29° Corresponding to the reflections from the (220), (311), (400), (422), (511), (440), and (533) can be easily indexed to the pure cubic inverse spinel structure of magnetite, which matches well with the reported data (JCPDS: 63-3107) [21]. The peaks are intense and well-defined, which suggests a good degree of structural order at long range. The XRD pattern of MGO during the adsorption-desorption process was similar to the XRD pattern of MGO, indicating the stability of the adsorbent during the adsorption process.

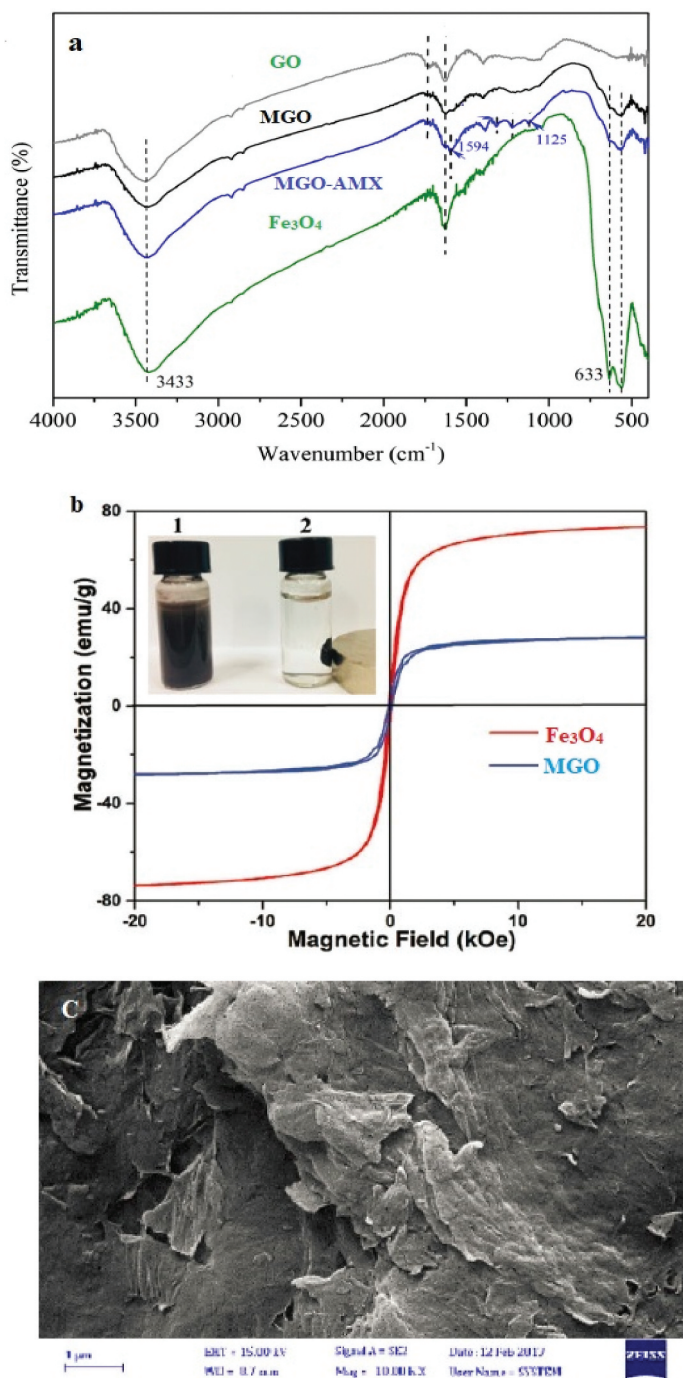


Figure 2. FT-IR image of as synthesised MGO and MGO-AMX(a); magnetic hysteresis loops of Fe_3O_4 and MGO (b); SEM images of GO (c) and MGO (d); TEM images of GO (e) and MGO (f); nitrogen adsorption – desorption isotherms of MGO (g).

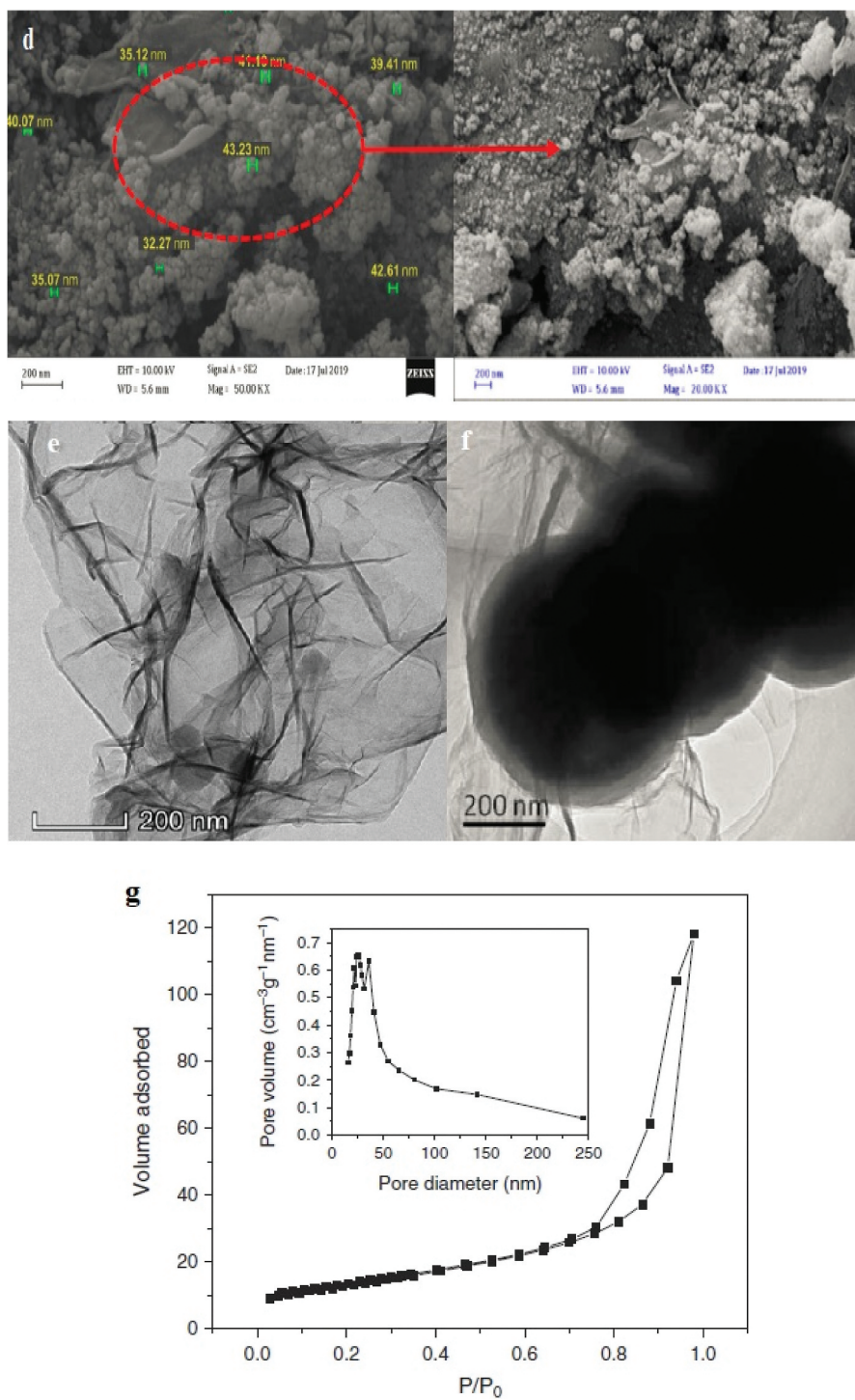


Figure 2. (Continued).

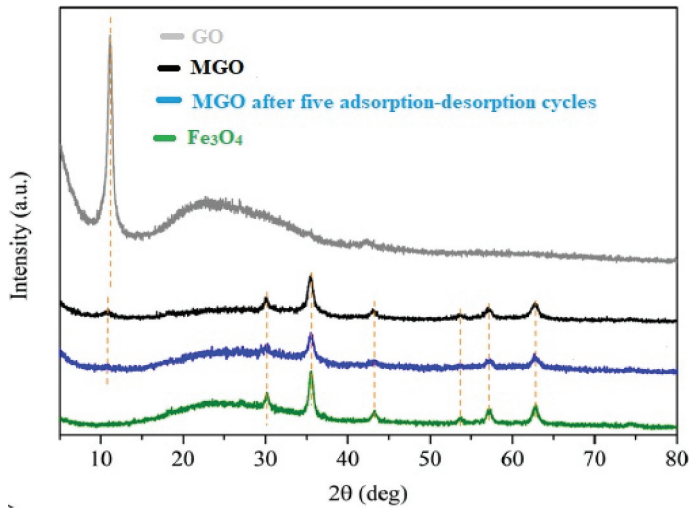


Figure 3. XRD patterns of GO, Fe₃O₄ NPs, and MGO samples before and after recycling.

3.2. Effect of parameters

The evaluation of changes in the adsorption capacity by changing contact time has been found to be important; thus, we conducted experiments related to AMX adsorption (Figure 4). The results were indicative of reaching the equilibrium after 90 min of the process. Moreover, higher adsorption was detected in the initial steps of the process, which is related to the existence of higher adsorption sites on the adsorbent initially [38,39]. After that, a drop in the AMX adsorption rate was recognised, which is explained based on the lack of sufficient vacant sites. As MGO adsorption sites were filled, a decline was recognised in the rate of transferring the AMX molecules from the exterior of active sites to their interior [40]. Our findings are in line with studies conducted by other researchers [41,42].

Considering available documents, three stages have been detected for the adsorption process onto porous solids; these three stages are as follows: 1) Boundary layer diffusion (or outer diffusion) in which external mass transfer of the adsorbate takes place from the liquid film to the exterior surface of adsorbent; 2) Intra-particle diffusion (or inner diffusion) in which the transport of adsorbate happens from the adsorbent exterior surface to pores or capillaries of the internal structure of adsorbent, and 3) The adsorbate adsorption is done on inner and outer active sites of the adsorbent [43]. In our study, AMX molecules are exposed to external sites of MGO directly; the AMX adsorption process is first done onto outside sites of MGO, and the process is then continued to interior sites by diffusion.

As another effective parameter on the efficiency of the studied process, the adsorbent mass was evaluated. As provided by Figure 5, for higher MGO mass, higher AMX removal efficiencies could be achievable; this is clearly related to the remarkable accessibility of adsorption sites [44]. It should be noted that we employed different masses (0.25–2.5 g/L). A substantial difference was detected in the efficiency of the system at an MGO mass of 1.5 g compared to other masses, which was our reason for selecting a mass of 1.5 g as the optimum MGO mass for utilising in the next laboratory tests.

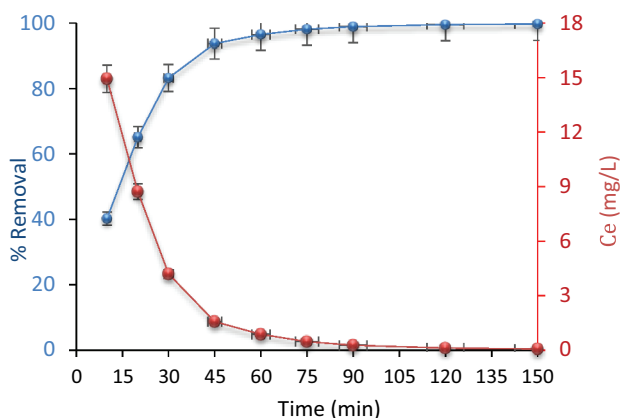


Figure 4. Amount of mixing time on the percentage of AMX removal ($C_0=25$ mg/L, pH=5, dose=1.5 g/L and 30°C).

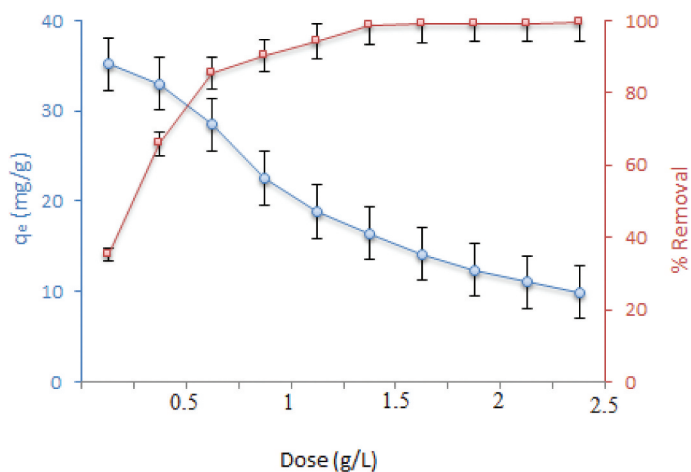


Figure 5. Amount of adsorbent efficacy on the percentage of AMX removal ($C_0=25$ mg/L, pH=5, 90 min and 30°C).

Another effective factor in the efficiency of the adsorption process introduced by previous studies is initial concentration; thus, its effect was also studied in our study (Figure 6). Considering the results, the AMX removal efficiency decreased at high concentrations. Based on the Figure, for higher concentrations of AMX, the equilibrium adsorption capacity (q_e) is developed, which might be due to enhancing the driving force for overcoming AMX resistance and developing mass transfer between the adsorbent and aqueous phase [45]. Our findings, in this case, were detected to be in accordance with similar studies [41,46].

The effects of solution pH on AMX removal by MGO are shown in Figure 7(a). As can be seen, the removal efficiency decreased with the increase of solution pH. MGO exhibited higher affinity for AMX at pH 3–5. This result suggested that the adsorption of AMX by MGO was highly pH-dependent. It also indicated that the graphite structures of the MGO

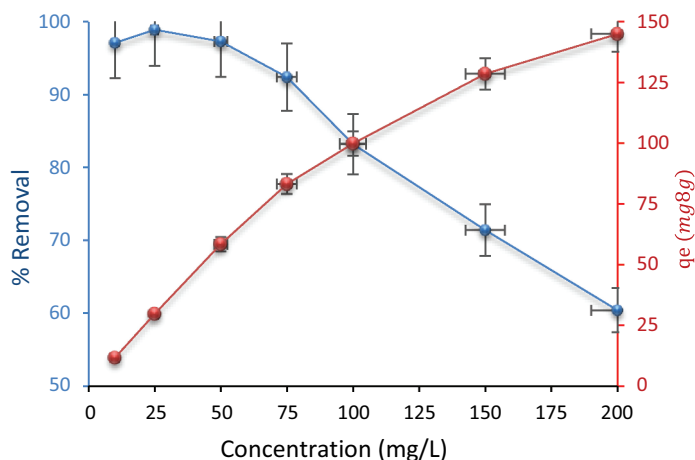


Figure 6. Effect of initial concentration on AMX removal (Dose: 1.5 mg/L, pH= 5, 90 min and 30°C).

played the predominant role in AMX adsorption. The variation of pH affected the surface charge of MGO and the species distribution of AMX in aqueous solution. MGO carried various oxygen-containing functional groups (e.g. $-\text{COOH}$ and $-\text{OH}$), which may change at different solution pH values. At acidic pH, most of these functional groups are protonated and presented the positively charged form. At higher pH, the MGO surface will become negatively charged due to the deprotonation of functional groups [21]. For MGO, the pH_{pzc} at which the net surface charge on the adsorbent is zero was obtained as 5.7 (Figure 7(b)). At $\text{pH} < \text{pH}_{\text{pzc}}$ and $\text{pH} > \text{pH}_{\text{pzc}}$, the adsorbent surface has a net positive charge and a net negative charge, respectively [46]. The protonation of hydroxyl ($-\text{OH}$) leads to generating cationic form ($-\text{OH}_2^+$) on the MGO surface is protonated, which results in the formation of electrostatic attraction between MGO and AMX anions; based on this, favourable AMX adsorption by studied adsorbent is recognised at acidic pH [10]. Nevertheless, deprotonation of the hydroxyl ($-\text{OH}$) to anionic form ($-\text{O}^-$) in the alkaline pH range leads to declining positively charged sites; this is not a suitable condition for the adsorption of AMX molecules, which have a negative charge and leads to declining adsorption capacity of AMX onto MGO. The observed result can be due to the fact that an electrostatic repulsion occurs between the sites with negative charges present on the adsorbent surface and the AMX molecules [11]. Thus, favourable AMX adsorption happens for the pH values lower than pH_{pzc} .

The effect of anions and cations on the removal efficiency of AMX is shown in Figure 7(c). It was found that the monovalent anions (Cl^- , NO_3^-) exhibited a lower influence on the adsorption capacity of AMX than that of divalent anions (SO_4^{2-}). This could be attributed to the fact that the divalent ions had stronger a squeezing-out effect due to their high polarising power. The adsorbed SO_4^{2-} might have hydration shells of dense water, which could impede the available adsorption sites by blocking the hydrophobic adsorption region. In addition, SO_4^{2-} , Cl^- , and NO_3^- might directly compete for adsorption sites due to inner-sphere complexation, which hinders the formation of charge-assisted H-bonds with antibiotics. The effect of cations (Mg^{2+} and Ca^{2+}) on AMX adsorption by MGO was

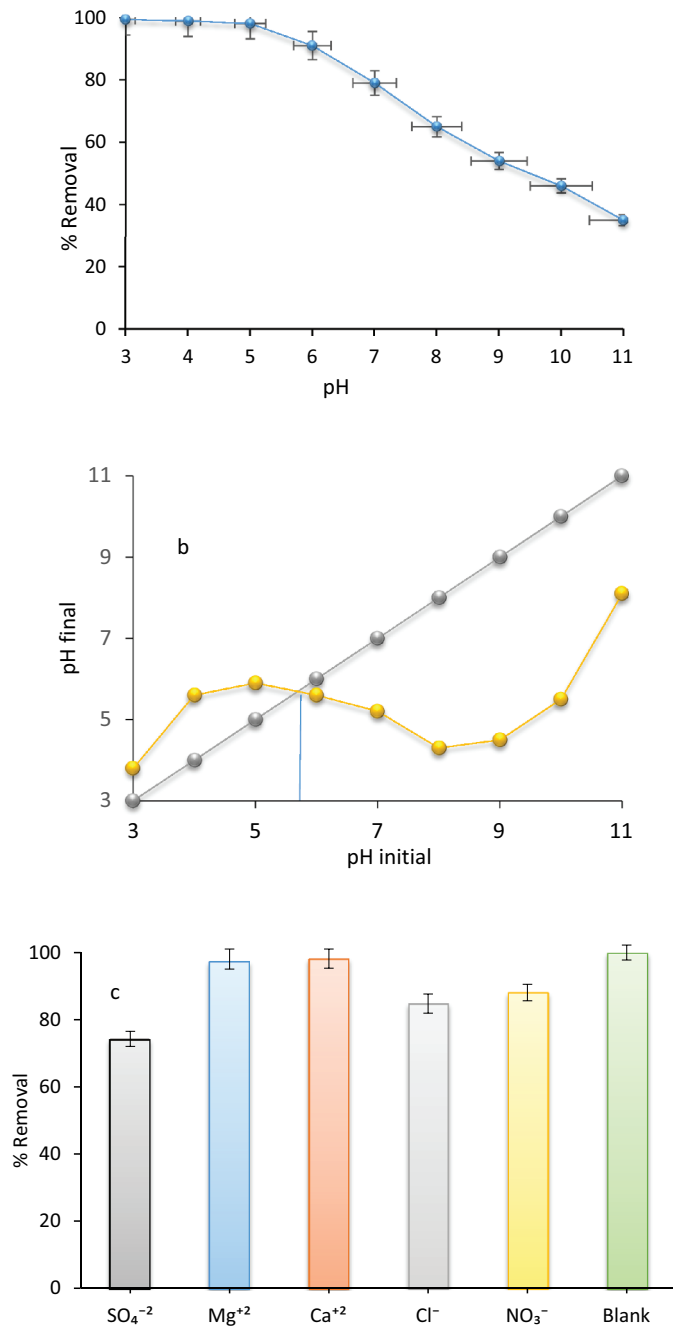


Figure 7. pH influence on the percentage of AMX removal (a); pH_{pzc} value of the adsorbent (b); effect of anions and cations on the removal efficiency (c).

detected to be insignificant. It can be attributed to the strong repulsion between the cations and the positively charged surface of MGO, resulting in minimal interference with the adsorption of AMX. It should be noted that the experiments were carried out at pH of 5, as the optimal pH.

3.3. Isotherm study

Conducting studies related to isotherm models has been found to be necessary for elucidating adsorption behaviour and providing data on mechanisms of adsorption [35]; thus, Langmuir, Freundlich, D-R, and Temkin adsorption isotherms were utilised for evaluating the AMX adsorption on MGO and obtaining the useful data in the studied process. Detailed information on the introduced models and obtained data from the models are provided in Table 2. The Langmuir equation involves four variables: q_e , which represents the adsorption capacity in milligrams per gram; C_e , which indicates the equilibrium concentration of AMX in the solution after adsorption in milligrams per litre; q_{max} , which denotes the maximum adsorption capacity in milligrams per gram, and K_L , which is the Langmuir constant [47]. To calculate K_L , one can plot $1/C_e$ against $1/q_e$. To determine the constants of the Freundlich model, i.e. K_F and $1/n$, a line is plotted by logging q_e against $\log C_e$ and then used for calculations. The Temkin equation unequivocally employs the variables of b , T , R , and K as definitive representations of the Temkin constant (J/mol) for adsorption heat, absolute temperature (K), gas constant (8.314 J/mol K), and the Temkin isotherm constant (L/g), respectively [48]. The D-R equation necessitates the use of four variables, namely q_e , q_m , K , and ϵ . These variables correspond to the adsorption capacity (mg/g), the maximum adsorption capacity (mg/g) achieved when the surface is fully coated, the parameter relevant to adsorption energy (mol^2/kJ^2), and the Polanyi potential ($\epsilon = RT \ln(1 + 1/C_e)$), respectively. The adsorption

Table 2. Results obtained from isotherm studied of AMX removal onto MGO.

Isotherm	Formula	Plot	parameter	Tem (°C)						
				20°C	30°C	40°C	50°C			
Langmuir	$\frac{C_e}{q_e} = \frac{1}{q_m K_L} + \frac{C_e}{q_m}$ $RL = \frac{1}{1 + KC_0}$	$\frac{C_e}{q_e}$ vs. C_e	q_{max}	91.4	103.9	112.3	122.5			
			K	0.027	0.044	0.071	0.095			
			R_L	0.127	0.108	0.068	0.041			
			R^2	0.994	0.997	0.994	0.992			
			SSE	0.793	0.811	1.25	1.63			
			SAE	0.411	0.872	0.927	1.34			
			ARE	1.14	0.947	1.96	0.772			
			ARS	0.743	0.952	0.674	1.39			
			Freundlich	$\text{Log} q_e = \log K_F + \frac{1}{n} \text{Log} C_e$	Log q_e vs. Log C_e	K_F	0.195	0.274	0.364	0.495
						n	2.17	2.95	4.51	3.82
R^2	0.914	0.902				0.858	0.894			
SSE	3.25	5.32				7.35	4.54			
SAE	2.76	7.36				5.64	5.39			
ARE	5.39	6.78				4.94	6.74			
ARS	8.21	5.58				9.29	4.56			
Temkin	$q_e = \frac{RT}{b} \ln(k_T C_e) \quad B = \frac{RT}{b}$	q_e vs. $\ln C_e$	K_T	0.814	0.924	1.06	1.28			
			B	30.25	26.54	19.81	11.73			
			R^2	0.926	0.929	0.917	0.906			
			SSE	9.24	6.35	7.11	9.25			
			SAE	7.32	6.45	11.2	7.79			
			ARE	9.73	7.96	4.63	7.34			
			ARS	4.39	9.82	5.37	5.31			
D-R	$\text{Ln} q_e = \text{Ln} q_m - K \epsilon^2 \quad E = \frac{1}{\sqrt{2K}}$	q_e vs. ϵ^2	q_m	48.27	53.18	56.21	59.35			
			E	1.68	2.15	3.125	5.88			
			R^2	0.747	0.795	0.781	0.786			
			SSE	4.32	8.56	11.5	7.14			
			SAE	7.25	6.34	7.65	9.34			
			ARE	9.36	5.72	4.68	5.46			
			ARS	6.25	9.31	5.36	4.75			

energy E (kJ/mol) gauges the free energy alteration required for a molecule to move from a solution to solid surfaces. To calculate K and q_m , a plot is generated with $\ln q_e$ vs. ϵ^2 , and the slope and intercept are then used [49]. Our analysis unmistakably shows that the Langmuir isotherm was the optimal model for fitting the experimental data, as demonstrated by Table 2. This fit was observed for all temperatures with the highest $R^2 = 0.992$ (Figure 8). In addition, the error functions for the Langmuir model are lower than other models. The mentioned results confirmed the suitability of the Langmuir isotherm model for the studied process; according to this model, our adsorption process was homogeneous and monolayer adsorption. In addition, based on Langmuir constants, the R_L is estimated; for this study, its value was between 1 and 0, which is representative of the favourable AMX adsorption. Calculating the n value is done based on the Freundlich model ($n > 1$); this parameter represents the intensity of the adsorption and heterogeneous surface of MGO for AMX adsorption. Considering the D-R model, a good fit with a precise explanation is achieved for the detected data. In addition, since the values less than 8 kJ/mol are obtained for activation energy, the physisorption is the type of studied adsorption process.

Considering the results of the isotherm study, the adsorption capacity of MGO was compared with that of other adsorbents in AMX removal. As reported in Table 3, the

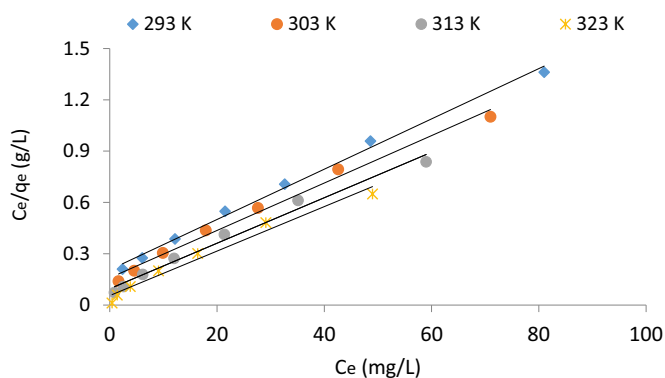


Figure 8. Langmuir adsorption isotherm of AMX on MGO.

Table 3. Comparison of adsorption capacity of different adsorbents for AMX removal.

Adsorbents	Condition	Q_m (mg/g)	Ref
AC-Jujube nuts	Time=90 min, pH=3, C_0 =20 mg/L, Dose=2 g/L, Tem=30°C	46.1	[1]
MWCNT ₅	Time=120 min, pH=5, C_0 =50 mg/L, Dose=1 g/L, Tem=25°C	68.2	[2]
AC- Cashew	Time=150 min, pH=5, C_0 =25 mg/L, Dose=1.5 g/L, Tem=25°C	71.9	[3]
AC- Date Pits	Time=90 min, pH=5, C_0 =10 mg/L, Dose=2 g/L, Tem=30°C	100.2	[8]
AC- Olive stone	Time=150 min, pH=7, C_0 =50 mg/L, Dose=3 g/L, Tem=25°C	70.3	[11]
Magnetic biochar	Time=210 min, pH=5, C_0 =10 mg/L, Dose=2.5 g/L, Tem=30°C	41.6	[27]
AC-nanofiber	Time=240 min, pH=3, C_0 =100 mg/L, Dose=1 g/L, Tem=25°C	65.2	[40]
Cellulose-flax noil	Time=300 min, pH=3, C_0 =25 mg/L, Dose=4 g/L, Tem=25°C	93.4	[41]
AC- Caesalpinia	Time=90 min, pH=5, C_0 =25 mg/L, Dose=2.5 g/L, Tem=30°C	78.9	[42]
Bentonite	Time=75 min, pH=7, C_0 =20 mg/L, Dose=1.2 g/L, Tem=30°C	87.6	[43]
Modified AC	Time=150 min, pH=7, C_0 =50 mg/L, Dose=2 g/L, Tem=50°C	56.4	[44]
Magnetic-AC	Time=200 min, pH=5, C_0 =100 mg/L, Dose=3 g/L, Tem=40°C	39.2	[50]
ACF/Fe ₃ O ₄	Time=90 min, pH=3, C_0 =25 mg/L, Dose=1.5 g/L, Tem=50°C	122.5	This study

adsorption capacity of MGO is good, and this adsorbent shows high adsorption compared to other adsorbents. Therefore, MGO is more effective than other adsorbents for AMX removal.

3.4. Adsorption kinetics

Kinetic models have been found to be applicable for ascertaining and controlling mechanisms of adsorption. The physical and chemical properties of adsorbent are the factors governing the mechanism of the process [50]. The PFO, PSO, and intra-particle diffusion models were the models employed in this study for assessing the kinetics and mechanism of AMX adsorption onto the adsorbent. The correlation coefficient (R^2) was used for defining the degree of the correlation of results observed in this section.

There was an enhancement in AMX adsorption for higher contact times; in higher contact times, mass transfer in the bulk solution resistance is developed to declining boundary layer resistance, and the kinetic energy of hydrated ions is developed, which are reasons for enhancing adsorption in higher times. In the case of the agitation time, its increase leads to reducing the boundary layer resistance and enhancing the mobility of ions in the solution [51].

The PFO, as an extensive model for the kinetic behaviour of adsorbent, assumes a direct proportion for the rate of changes in the solute with the changes in the saturation concentration and the consumed level of adsorbent against time. The expression of the PFO rate equation is as follows [52]:

$$\text{Log}(q_e - q_t) = \text{log } q_e - \frac{k_1}{2.303} t \quad (7)$$

In the mentioned equation, q_e has been introduced as the adsorption capacity at time t (mg/g), and k_1 (min^{-1}) was the PFO rate constant. Calculating the rate constant (k_1) and correlation coefficients were considered for different concentrations of the AMX; this is done based on the linear plots of $\text{log}(q_e - q_t)$ against t (Figure 9(a) and Table 4). Data obtained from PFO was representative of very good correlation coefficients for the studied concentrations. However, the fit of PFO to the experimental data was detected to be poor, which is approved based on the presence of a remarkable difference in equilibrium adsorption capacity (q_t) between the experiments and calculations.

The linear form of PSO is as follows [53]:

$$\frac{t}{q_t} = \frac{1}{h} + \frac{t}{q_e} \quad (8)$$

In the above equation, for $t \rightarrow 0$, $h = k_2 q_e^2$ (mg/g.min) could be indicative of the initial adsorption rate, and k signifies the PSO rate constant (g/mg.min). For the applicability of PSO, we should obtain a straight line from plotting t/q_e versus t ; the slope and intercept of the plot are used for calculating q_e and k , respectively. The plots of the linearised form of the PSO reaction at different AMX concentrations are shown in Figure 9(b). Moreover, in Table 4, the rate constants of PFO and PSO and the corresponding correlation coefficients are represented. As depicted, good straight lines ($R^2 > 0.99$) are obtained

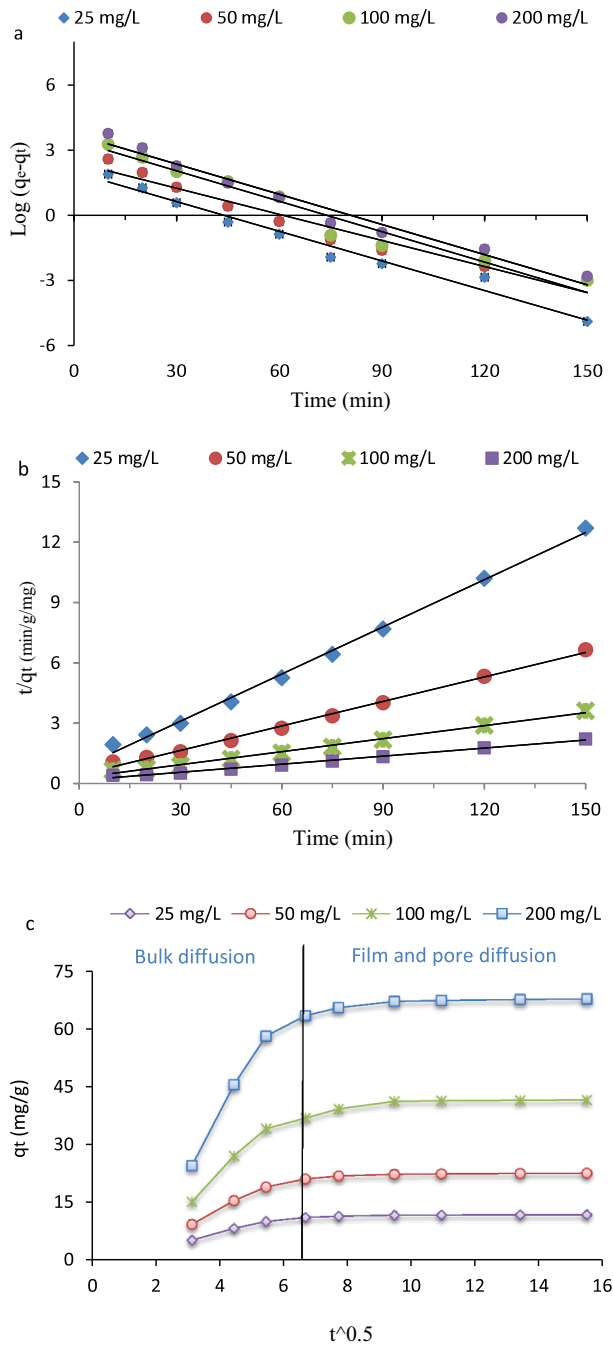


Figure 9. PFO plot (a); PSO plot (b); IPD plot (c) kinetic models for AMX adsorption on the MGO.

based on the PSO model; the rate constant for this model was detected to be 0.0011–0.0083 g/mg-min, and theoretical values of q_e obtained by this model had a thriving agreement with its experimental values. In addition, the error functions detected for the PSO were lower than that of PFO.

Table 4. Kinetic parameters for the adsorption of AMX on MGO.

Model	Parameters	Concentration (mg/L)			
		25	50	100	200
PFO	$Q_{(cal)}$	4.72	14.3	35.9	71.3
	K_1	0.103	0.092	0.064	0.042
	R^2	0.975	0.949	0.958	0.971
	SSE	6.21	7.36	6.23	7.32
	SAE	5.23	5.68	4.72	3.45
	ARE	7.25	7.34	8.96	8.36
	ARS	9.72	9.32	4.39	5.95
	$Q_e (cal)$	12.84	35.9	71.2	117.3
PSO	K_2	0.0083	0.0037	0.0015	0.0011
	R^2	0.999	0.995	0.996	0.992
	SSE	1.25	0.945	0.679	1.15
	SAE	0.689	1.35	1.49	0.897
	ARE	1.02	0.746	0.789	0.954
	ARS	1.74	1.59	0.697	1.28
	Stage 1				
	K_1	17.4	14.2	12.3	11.8
IPD	I	4.02	7.25	11.2	25.4
	R^2	0.962	0.993	0.992	0.998
	Stage 2				
	K_2	2.25	1.95	1.62	1.22
	I	2.97	5.24	8.67	21.2
	R^2	0.964	0.991	0.985	0.971

3.5. Intraparticle diffusion model

Equation of this model is shown as below [54]:

$$q_t = Kt^{0.5} + I \quad (9)$$

In the above equation, K [$\text{mg}/(\text{g}\cdot\text{min}^{0.5})$] and I (mg/g) are representative of the IPD rate constant and the constant related to the thickness of the boundary layer, respectively. Calculating K and I are done using the line obtained by plotting q_t vs. $t^{0.5}$ (Figure 9(c)); the obtained values are seen in Table 3. Considering the plots in Figure 9(c), two different portions are clearly detectable. It confirms that adsorption is done in different stages; based on this, there is a larger slope portion (the diffusion of adsorbate to the external surface of adsorbent) and a smaller slope portion (the gradual adsorption stage related to the diffusion of adsorbate molecules inside the adsorbent pores) [55,56]. In the case of linearity of the plot of q_t versus $t^{0.5}$ and its passing through the origin ($I = 0$), there is only one rate-limiting step, i.e. IPD. Lack of passing through the origin is indicative of participation of IPD along with other factors in the adsorption. Based on intercept (I) values, a concept is provided for the thickness of the boundary layer; when there is a great value for the I , a higher effect is offered by the boundary layer. Increasing initial AMX concentrations (10–200 mg/L) leads to enhancing the I values, which is indicative of the remarkable effect of initial AMX concentration on developing boundary layer diffusion effect [57,58].

3.6. Thermodynamic studies

By conducting these studies, the nature of the process (if it is spontaneous or not) and its applicability is determined by estimating actual parameters, i.e. ΔG° (kJ/mol), ΔH° (kJ/mol),

Table 5. Values of thermodynamic parameters for the adsorption of AMX onto MGO.

Temperature (K)	ΔG^0 (kJ/mol)	ΔH^0 (kJ/mol)	ΔS^0 (kJ/mol K)
293	-3.802		
303	-4.806	38.2	0.354
313	-6.391		
323	-10.72		

ΔS^0 (kJ/(mol.K)); this aim was achieved based on the experiments conducted at 293–323 K. Estimating above-mentioned parameters was done based on Equations (10)–(12) [59]:

$$\Delta G^0 = -RT \ln K \quad (10)$$

$$K = \frac{q_e}{C_e} \quad (11)$$

In cited equations, T is absolute temperatures (K), and K is the apparent equilibrium constant. Van't Hoff equation (shown below) was utilised for estimating ΔH^0 and ΔS^0 at different temperatures [60]:

$$\ln(K) = \frac{\Delta S^0}{R} - \frac{\Delta H^0}{RT} \quad (12)$$

According to Table 5 (values obtained for mentioned parameters), an endothermic nature was detected for the adsorption of AMX, based on positive ΔH^0 values. Moreover, ΔS^0 obtained for the AMX adsorption process was positive; this is representative of the fact that, during the adsorption, the randomness at the MGO – solution interface is associated with an irregular increase [61]. In addition, ΔG^0 with negative values is indicative of a spontaneous adsorption process on MGO [62,63]. Moreover, at higher temperatures, less favourable adsorption was detectable, which could be explained based on the decrease of ΔG^0 values with the increase in temperature [64].

3.7. Regeneration process

One of the important parameters in the field of adsorbing pollutants is the economic issue, which can be economically justified by recycling and reusing the adsorbent. Regeneration of the adsorbent was conducted using the peroxymonosulfate (PMS) oxidation method. For this purpose, after adsorbing 25 mg/L AMX in a 100 mL solution, the used adsorbent was separated using a magnet. It was then exposed to 2 mM PMS for 2 hours and rinsed with 100 mL of distilled water to remove any remaining PMS. Finally, it was dried in an oven at 103°C for 2 hours before proceeding with the next step of the test. In this study, using the parameters optimised in the previous stages, adsorption and desorption tests were performed in six stages, and the results are shown in Figure 10; as seen, in the first stage, at a concentration of 25 mg/L, 100% of AMX is separated from the aqueous solution, and after six times of recovery and re-adsorption, the removal rate reaches 87.9%. The decrease in the amount of adsorption in different stages is due to the decrease in the amount of adsorbent in the collection stage. In each stage, about 4% of MGO is reduced, that is, 96% of the adsorbent used in the first stage is present in the

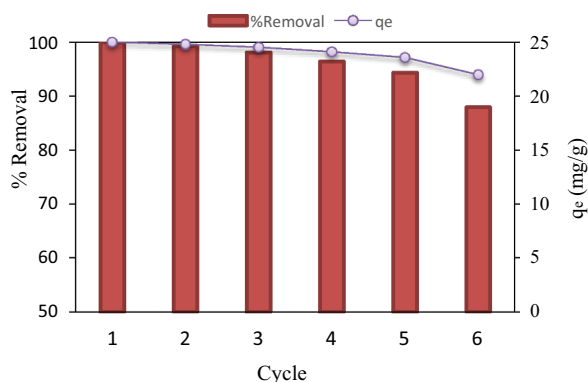


Figure 10. Reuse of MGO in AMX removal under conditions: (initial AMX concentration: 25 mg/L; adsorbent dose: 1.5 g/L; contact time: 90 min; pH: 5 and temperature: 30°C).

second stage. Also, it may be attributed to the fact that the adsorbent active sites are not empty; some of the surface active sites that were saturated in the first stage remain the same during the washing step with distilled water [65,66].

GO alone is also a good adsorbent, and in our tests, it was able to remove 96.1% of AMX within 90 min, but the main problem with GO is its collection. Only in the second stage, we could collect only 69% of the adsorbent, which is a very small amount considering the MGO (96%).

3.8. Adsorption mechanisms

The mechanism of adsorption of AMX on MGO adsorbent is due to intraparticle diffusion and It confirms that adsorption is done in different stages; based on this, there is a larger slope portion (Bulk diffusion) and a smaller slope portion (Film and pore diffusion). Also Briefly, the active functional groups in MGO such as $-OH$ and $-C=O$ groups can form covalent or non-covalent (hydrogen bonding, ionic interaction, $\pi-\pi$ stacking, etc.) while the $-NH_2$ groups can interact with covalent (imine bonds), non-covalent interaction and semi-covalent (amide bonds) with the MGO molecules (Figure 11).

4. Conclusion

The AMX adsorption onto MGO was appraised in the present study. For the mentioned adsorbent, well dispersion in water and easy separation from water using an external magnetic field were clearly detectable. In assessing the efficiency of the studied process, initial AMX concentration, MGO mass, temperature, and initial pH were found to be the factors that are effective on the efficiency of the AMX adsorption. The PSO was the more suitable model for AMX adsorption by MGO, and the Langmuir could exhibit the best potential to fit the detected data. For MGO, the value of 122.5 mg/g was the maximum adsorption capacity, which was obtained at 50°C. The studied process was recognised to be spontaneous, endothermic, and physisorption, which was determined based on the observed values for thermodynamic parameters. Furthermore, the acidic condition was found to be effective in the progression of the AMX adsorption efficiency. Thus, based

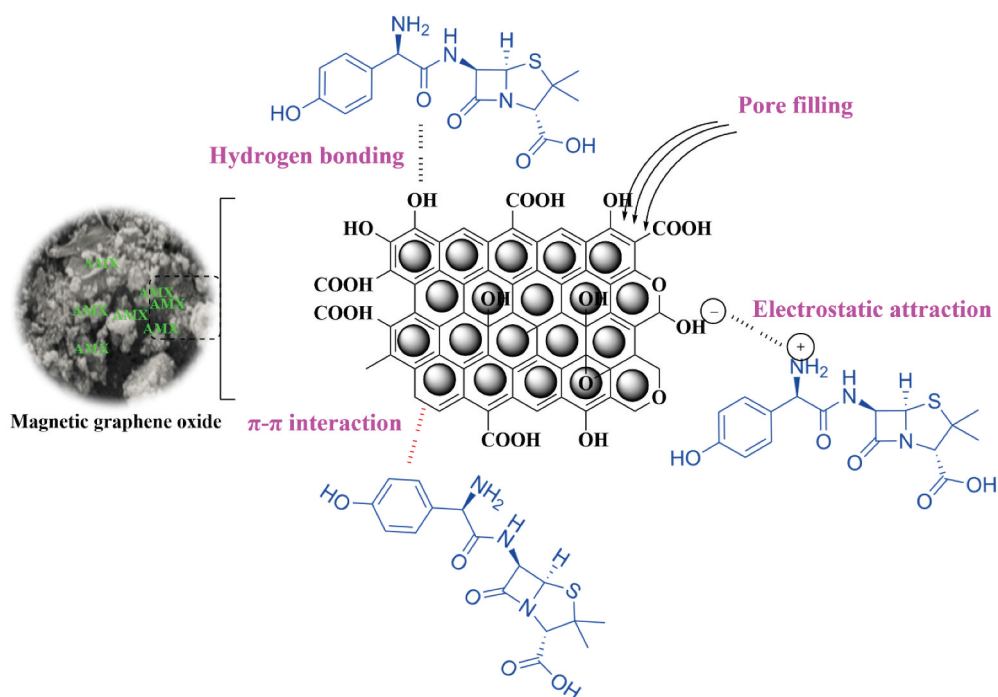


Figure 11. Adsorption mechanism of AMX onto MGO.

on the data obtained from different sections of the present study, a bright future might be anticipated for the application of MGO as an adsorbent for sufficient treatment of wastewater containing antibiotics.

Acknowledgments

The authors would like to thank Zahedan University of Medical Sciences for financial support and assistance in performing the experimental work of this research (code: 10490).

Disclosure statement

No potential conflict of interest was reported by the author(s).

References

- [1] Y. Belaissa, F. Saib and M. Trari, *Reac. Kinet. Mech. Cat.* **135**, 1011–1030 (2022). doi:10.1007/s11144-022-02159-0.
- [2] D. Balarak, F.K. Mostafapour, E. Bazrafshan and T.A. Saleh, *Water Sci. Technol.* **75**, 1599–1606 (2017).
- [3] D.R. Lima, E.C. Lima and C.S. Umpierrez, *Environ. Sci. Pollut. Res.* **26**, 16396–16408 (2019). doi:10.1007/s11356-019-04994-6.
- [4] J. Leonard, M. Githinji, M.K.M. Ramble and O. Ankumah, *Water Air Soil Pollut.* **21** (9), 191–201 (2011).

- [5] M. Ibáñez, L. Bijlsma, E. Morales, L. Pastor and F. Hernández, *J. Hazard. Mater.* **260**, 389–398 (2013). doi:10.1016/j.jhazmat.2013.05.023.
- [6] X. Bian, T. Zhan, L. Wang, W. Zhou and Q. Dai, *Chemosphere* **233**, 762–770 (2019).
- [7] N. Olama, M. Dehghani and M. Malakootian, *Appl. Water Sci.* **8**, 97 (2018). doi:10.1007/s13201-018-0733-7.
- [8] M. Belhachemi and S. Djelaila, *Environ. Process* **4**, 549–561 (2017).
- [9] A. Boukhelkhal, O. Benkortbi and M. Hamadeche, *Water Air Soil Pollut.* **226**, 323 (2015). doi:10.1007/s11270-015-2587-z.
- [10] A. Moarefian, H.A. Golestani and H. Bahmanpour, *J. Environ. Health Sci. Eng.* **12**, 127 (2014). doi:10.1186/s40201-014-0127-1.
- [11] L. Limousy, I. Ghouma and A. Ouederni, *Environ. Sci. Pollut. Res.* **24**, 9993–10004 (2017). doi:10.1007/s11356-016-7404-8.
- [12] J. Berges, S. Moles and M.P. Ormad, *Environ. Sci. Pollut. Res.* **28**, 8442–8452 (2021).
- [13] H. Li, J. Hu and C. Wang, *Water Air Soil Pollut.* **228**, 201 (2017). doi:10.1007/s11270-017-3385-6.
- [14] M. Malakootian, M. Yaseri and M. Faraji, *Environ. Sci. Pollut. Res.* **26**, 8444–8458 (2019). doi:10.1007/s11356-019-04227-w.
- [15] Q. Li, R. Jia, J. Shao and Y. He, *J. Clean. Prod.* **209**, 755–761 (2019). doi:10.1016/j.jclepro.2018.10.183.
- [16] S. Li, X. Zhang and Y. Huang, *J. Hazard. Mater.* **321**, 711–719 (2017).
- [17] D. Li, X. Guo, H. Song, T. Sun and J. Wan, *J. Hazard. Mater.* **351**, 250–259 (2018). doi:10.1016/j.jhazmat.2018.03.007.
- [18] Y. Shi, H. Wang and G. Song, *Environ. Sci. Pollut. Res.* **29**, 30774–30789 (2022). doi:10.1007/s11356-021-17654-5.
- [19] F. Sun, Y. Zhu, X. Liu and Z. Chi, *Environ. Sci. Pollut. Res.* **30**, 27560–27569 (2023). doi:<https://doi.org/10.1007/s11356-022-24226-8>.
- [20] D.R. Rout and H.M. Jena, *Environ. Sci. Pollut. Res.* **29**, 32105–32119 (2022). doi:10.1007/s11356-021-17944-y.
- [21] W.M.A. El-Rouby, A.A. Farghali and M.A. Sadek, *J. Inorg. Organomet. Polym.* **28**, 2336–2349 (2018). doi:10.1007/s10904-018-0885-9.
- [22] A.S. Eltaweil, E.M. Abd El-Monaem and G.M. El-Subruiti, *J. Porous Mater.* **30**, 607–618 (2023). doi:10.1007/s10934-022-01347-6.
- [23] F. Najafi, *Int. Nano Lett.* **5**, 171–178 (2015). doi:10.1007/s40089-015-0151-x.
- [24] J.T. Martins, C.H. Guimarães, P.M. Silva, R.L. Oliveira and P. Prediger, *Environ. Sci. Pollut. Res.* **28**, 3386–3405 (2021). doi:10.1007/s11356-020-10779-z.
- [25] T.J. Al-Musawi, A.H. Mahvi, A.D. Khatibi and D. Balarak, *J. Porous Mat.* **28**, 835–852 (2021). doi:10.1007/s10934-021-01039-7.
- [26] P. Prarat, P. Hongsawat and P. Punyapalukul, *Environ. Sci. Pollut. Res.* **27**, 6560–6576 (2020). doi:10.1007/s11356-019-07186-4.
- [27] R. Li, Z. Wang and X. Zhao, *Environ. Sci. Pollut. Res.* **25**, 31136–31148 (2018). doi:10.1007/s11356-018-3064-1.
- [28] X. Kong, Y. Liu and J. Pi, *Environ. Sci. Pollut. Res.* **24**, 6679–6687 (2017). doi:10.1007/s11356-017-8376-z.
- [29] H.R. Nodeh, W.A.W. Ibrahim, I. Ali and M.M. Sanagi, *Environ. Sci. Pollut. Res.* **23** (10), 9759–9773 (2016).
- [30] D.N. Shan, S.B. Deng, T.N. Zhao and B. Wang, Y. Wang, *J. Hazard. Mater.* **305**, 156–163 (2016). doi:10.1016/j.jhazmat.2015.11.047.
- [31] X.K. Tian, W.K. Wang, N. Tian, C.X. Zhou, C. Yang and S. Komarneni, *J. Hazard. Mater.* **309**, 151–156 (2016). doi:10.1016/j.jhazmat.2016.01.081.
- [32] S.Y. Wang, Y.K. Tang, K. Li, Y.Y. Mo and H.F. Li, *Bioresour. Technol.* **174**, 67–73 (2014).
- [33] H. Liang, C. Zhu and S. Ji, *Biochar.* **4** (3) (2022). doi:10.1007/s42773-021-00130-1.
- [34] L. Fang, Y. Miao, D. Wei and Y. Zhang, *Chemosphere* **262**, 128032 (2021). doi:10.1016/j.chemosphere.2020.128032.
- [35] W. Gege, M. Jiping, L. Shuang, G. Jing and J. Bo, *J. Colloid Interface Sci.* **528**, 360–371 (2018). doi:10.1016/j.jcis.2018.05.105.

- [36] X. Li, C. Wang, J. Zhang, J. Liu and B. Liu, *Sci. Total Environ.* **711**, 134847 (2020).
- [37] N. Li, M. He, X. Lu, L. Liang and R. Li, *Sci. Total Environ.* **761**, 143268 (2021).
- [38] D. Shan, S. Deng, T. Zhao, B. Wang, Y. Wang, J. Huang, G. Yu, J. Winglee and M.R. Wiesner, *J. Hazard. Mater.* **305**, 156–163 (2016). doi:10.1016/j.jhazmat.2015.11.047.
- [39] H.A. Alalwan, A.H. Alminshid, M.M. Mohammed, M.F. Mohammed and M.H. Shadhar, *Pollution* **8** (3), 995–1013 (2022).
- [40] J.M. Chaba and P.N. Nomngongo, *Emerg. Contam.* **5**, 143–149 (2019). doi:10.1016/j.emcon.2019.04.001.
- [41] H. Dongying and W. Lijuan, *J. Taiwan Inst. Chem. Eng.* **64**, 227–234 (2016). doi:10.1016/j.jtice.2016.04.028.
- [42] F.M. Kasperiski, E.C. Lima and C.S. Umpierrez, *J. Cleaner Prod.* **197**, 919–929 (2018). doi:10.1016/j.jclepro.2018.06.146.
- [43] E.K. Putra, R. Pranowo and J. Sunarso, *Water Res.* **43**, 2419–2430 (2009). doi:10.1016/j.watres.2009.02.039.
- [44] L. Sellaoui, E.C. Lima, G.L. Dotto and A.B. Lamine, *J. Mol. Liq.* **234**, 375–381 (2017). doi:10.1016/j.molliq.2017.03.111.
- [45] A.H. Mahvi and F.K. Mostafapour, *Fresenius Environ. Bull.* **27** (8), 5759–5767 (2018).
- [46] D. Balarak, Z. Taheri, M.J. Shim, S.M. Lee and C. Jeon, *Desalin. Water Treat.* **215**, 183–193 (2021). doi:10.5004/dwt.2021.26860.
- [47] J. Abdi and H. Abedini, *Chem. Eng. J.* **400**, 125862 (2020). doi:10.1016/j.cej.2020.125862.
- [48] J. Abdi, N.M. Mahmoodi, M. Vossoughi and I. Alemzadeh, *Microporous Mesoporous Mater.* **273**, 177–188 (2019). doi:10.1016/j.micromeso.2018.06.040.
- [49] Z. Rahmati, J. Abdi, M. Vossoughi and I. Alemzadeh, *Environ. Res.* **188**, 109555 (2020). doi:10.1016/j.envres.2020.109555.
- [50] C. Saucier, P. Karthickeyan and V. Ranjithkumar, *Environ. Sci. Pollut. Res.* **24**, 5918–5932 (2017). doi:10.1007/s11356-016-8304-7.
- [51] J. Abdi, M. Vossoughi, N.M. Mahmoodi and I. Alemzadeh, *Ultrason. Sonochem.* **39**, 550–564 (2017). doi:10.1016/j.ultsonch.2017.04.030.
- [52] J. Abdi, M. Vossoughi, N.M. Mahmoodi and I. Alemzadeh, *Chem. Eng. J.* **326**, 1145–1158 (2017). doi:10.1016/j.cej.2017.06.054.
- [53] D. Balarak, A.H. Mahvi, M.J. Shim and S.M. Lee, *Desalin. Water Treat.* **212**, 390–400 (2021). doi:10.5004/dwt.2021.26603.
- [54] S. Ahmadi, A. Banach and F.K. Mostafapour, *Desalin. Water Treat.* **89**, 297–303 (2017). doi:10.5004/dwt.2017.21362.
- [55] M. Yilmaz, T.J. Al-Musawi and M.K. Saloot, *Biomass Conv. Bioref.* **2022**. doi:10.1007/s13399-021-02279-y
- [56] T.J. Al-Musawi, N. Mengelizadeh and M. Taghavi, *Biomass Conv. Bioref.* **13**, 12179–12191 (2023). doi:10.1007/s13399-021-01962-4.
- [57] N.M. Mahmoodi and J. Abdi, *J. Ind. Eng. Chem.* **80**, 606–613 (2019). doi:10.1016/j.jiec.2019.08.036.
- [58] J. Abdi, M. Hadipoor, F. Hadavimoghaddam and A. Hemmati-Sarapardeh, *Chemosphere* **287**, 132135 (2022). doi:10.1016/j.chemosphere.2021.132135.
- [59] H. Azarpira, Y. Mahdavi and O. Khaleghi, *Pharm. Lett.* **8** (11), 107–113 (2016).
- [60] M.Y. Nassar, I.S. Ahmed and M.A. Raya, *J. Mol. Liq.* **282**, 251–263 (2019). doi:10.1016/j.molliq.2019.03.017.
- [61] G. Moghadam, J. Abdi, F. Banisharif, A. Khataee and M. Kosari, *J. Mol. Liq.* **341**, 117323 (2021). doi:10.1016/j.molliq.2021.117323.
- [62] K.R. Thines, E.C. Abdullah and N.M. Mubarak, *Renew. Sustain. Energy. Rev.* **67**, 257–276 (2017). doi:10.1016/j.rser.2016.09.057.
- [63] D. Balarak, F.K. Mostafapour and H. Azarpira, *Inter. J. Pharm. Technol.* **8** (3), 16664–16675 (2016).
- [64] R.A. Dyanati, Z.A. Yousefi, J.Y. Cherati, *J. Mazand. Uni. Med Sci* **22** (SUPPL. 2), 13–20 (2013).
- [65] R.A. Dyanati-Tilaki, Z. Yousefi, *J. Yazdani-Cherati, J. Mazand. Uni. Med. Sci.* **23** (106), 140–146 (2013).
- [66] H. Azarpira and Y. Mahdavi, *Pharm. Chem.* **8** (12), 61–67 (2016).